Published April 26, 2004

G-protein–gated TRP-like Cationic Channel Activated by Muscarinic Receptors: Effect of Potential on Single-channel Gating

Alexander V. Zholos,[1,3] Andrey A. Zholos,[2] and Thomas B. Bolton[3]

[1]Laboratory of Molecular Pharmacology of Cellular Receptors and Ion Channels, A.A. Bogomoletz Institute of Physiology, Kiev, 01024 Ukraine

[2]Department of Economical Cybernetics, Taras Shevchenko National University, Kiev, 01033 Ukraine

[3]Pharmacology and Clinical Pharmacology Basic Medical Sciences, St. George's Hospital Medical School, London SW17 ORE, UK

ABSTRACT There is little information about the mechanisms by which G-protein–coupled receptors gate ion channels although many ionotropic receptors are well studied. We have investigated gating of the muscarinic cationic channel, which mediates the excitatory effect of acetylcholine in smooth muscles, and proposed a scheme consisting of four pairs of closed and open states. Channel kinetics appeared to be the same in cell-attached or outside-out patches whether the channel was activated by carbachol application or by intracellular dialysis with GTPγS. Since in the latter case G-proteins are permanently active, it is concluded that the cationic channel is the major determinant of its own gating, similarly to the K_{ACh} channel (Ivanova-Nikolova, T.T., and G.E. Breitwieser. 1997. *J. Gen. Physiol.* 109:245–253). Analysis of adjacent-state dwell times revealed connections between the states that showed features conserved among many other ligand-gated ion channels (e.g., nAChR, BK_{Ca} channel). Open probability (P_O) of the cationic channel was increased by membrane depolarization consistent with the prominent U-shaped I-V relationship of the muscarinic whole-cell current at negative potentials. Membrane potential affected transitions within each closed-open state pair but had little effect on transitions between pairs; thus, the latter are likely to be caused by interactions of the channel with its ligands, e.g., Ca^{2+} and Gαo-GTP. Channel activity was highly heterogeneous, as was evident from the prominent cycling behavior when P_O was measured over 5-s intervals. This was related to the variable frequency of openings (as in the K_{ACh} channel) and, especially, to the number of long openings between consecutive long shuttings. Analysis of the underlying Markov chain in terms of probabilities allowed us to evaluate the contribution of each open state to the integral current (from shortest to longest open state: 0.1, 3, 24, and 73%) as P_O increased 525-fold in three stages.

KEY WORDS: Markov chain • channel kinetics • G-protein • carbachol • smooth muscle

INTRODUCTION

Many cell-surface receptors perform their intracellular communication functions by changing the activity, either opening or closing, of various ion channels. Mechanisms of gating of some ionotropic receptors in which agonist binding site(s) and ion channel pore are located within the same protein complex are now well understood, particularly in the case of the skeletal muscle nicotinic acetylcholine receptor (nAChR) (Edmonds et al., 1995). Appropriate models have been developed as an extension of an early scheme of del Castillo and Katz (1957) that now provide a physically realistic picture of how ligand binding could change receptor-conducting conformation (Colquhoun and Sakmann, 1998). These reaction mechanisms, also often referred to as kinetic models of ion channels, allow a physically meaningful interpretation of single-channel activity and a useful explanation of the whole-cell current behavior and physiological function (Pallotta, 1997).

The much larger and diverse superfamily of seven transmembrane spanning receptors produce signals to a variety of effectors, e.g., enzymes and ion channels, via G-proteins (for reviews see Gilman, 1987; Wickman and Clapham, 1995). However, much less is known about the interactions and mechanisms which lead to channel opening in these complex multi-component signaling systems.

One level of complexity arises due to the multisignaling nature of G-protein–coupled receptors (GPCRs), since both Gα-GTP and Gβγ subunits may have separate, sometimes opposite, functions (Hamm, 1998). An added level of complexity arises as multiple receptor subtypes for the same agonist are often coexpressed in the same tissue. These can converge to activate the

Address correspondence to Alexander V. Zholos, Laboratory of Molecular Pharmacology of Cellular Receptors and Ion Channels, A.A. Bogomoletz Institute of Physiology, Kiev, 01024 Ukraine. Fax: (044) 256 2000; email: zholosa@sghms.ac.uk

Abbreviations used in this paper: ACh, acetylcholine; GPCR, G-protein–coupled receptor; mAChR, muscarinic receptor; nAChR, nicotinic acetylcholine receptor; TRP, transient receptor potential.

Published April 26, 2004

same channel in a subtype-specific manner depending on which type of G-protein is involved.

The muscarinic receptor–operated cationic channel, the subject of our present study, exemplifies such complexity of GPCR signal transduction. This cationic channel is widely expressed in various smooth muscle tissues such as the gastrointestinal tract and airways, where it mediates the excitatory action of acetylcholine (ACh). Two muscarinic receptor (mAChR) subtypes, M2 and M3, are colocalized in the same tissues (Eglen et al., 1996). We found that although M2 receptor activation primarily causes activation of the channel, the M3 subtype plays an important "permissive" role (Bolton and Zholos, 1997; Zholos and Bolton, 1997). Thus, both receptor subtypes control the channel opening. Further studies have shown that, consistent with early reports of the inhibitory action of Pertussis toxin treatment on the mAChR cationic current (mI_{CAT}) (Inoue and Isenberg, 1990a; Komori and Bolton, 1990), the channel is coupled to the muscarinic receptor via Gαo protein (presumably an M2 effect) (Yan et al., 2003), whereas PLC inhibition also abolishes mI_{CAT} (presumably an M3 effect) (Zholos et al., 2004).

Furthermore, intracellular Ca^{2+} was shown to have both a permissive and a potentiating effect on channel opening (Inoue and Isenberg, 1990c; Wang et al., 1997); hence, a rise in $[Ca^{2+}]_i$ is necessary but not sufficient to activate mI_{CAT}. This results in a close, almost mirror, correlation between $[Ca^{2+}]_i$ level and whole-cell current amplitude (Pacaud and Bolton, 1991; Komori et al., 1993; Gordienko et al., 1999).

Moreover, the current shows an intrinsic voltage-dependent behavior (Benham et al., 1985; Inoue and Isenberg, 1990b), such that in the presence of the agonist membrane hyperpolarization can strongly attenuate the current, but in its absence even strong depolarization does not produce any detectable channel activation. A close and intriguing relationship exists between G-protein control and intrinsic voltage dependence of this channel. Thus, increasing the agonist concentration shifts the activation curve up to 40 mV negatively (Zholos and Bolton, 1994), whereas desensitization has an opposite effect (Zholos and Bolton, 1996). Membrane depolarization, in turn, has a strong sensitizing effect on channel opening (e.g., shifting the membrane potential from −50 to 50 mV reduces the carbachol EC_{50} value 20-fold), reduces latency of the response from 380 to 160 ms, and accelerates on-rate and decelerates off-rate during fast agonist application and removal (Bolton and Zholos, 2003).

These various observations at present are hard to reconcile within a general mechanism. The major obstacle is the lack of information on single-channel gating. In earlier reports, this cationic channel proved to be difficult to investigate in excised membrane patches. Therefore, channel activity was resolved in the so-called "magnified whole-cell mode" (Inoue et al., 1987; Kang et al., 2001), which provided initial valuable information on channel conductance, selectivity, and voltage dependence of its open probability (P_O), but channel kinetic states still needed to be studied at higher resolution. At present only a simplified two-state model is available (Inoue et al., 1987; Inoue and Isenberg, 1990b).

Here, we sought to answer—by studying single cationic channel kinetics—the many questions that arise due to the complex nature of whole-cell mI_{CAT}. This analysis was significantly facilitated by the possibility of obtaining outside-out patches in which only one channel was present. Our analysis revealed that channel activity was much more complex than previously thought, e.g., at least four open and four closed states exist with additional flicker and inactivated states. The molecular structure of this cationic channel remains incompletely defined but it may be a homo- or a heteromultimer of transient receptor potential (TRP) proteins (Walker et al., 2001; Lee et al., 2003). For this novel family of channel proteins the gating stimuli and mechanisms remain largely unknown (Clapham, 2003). We found that cationic channel activity consists of bursts of short, intermediate, and long openings with strong correlations between adjacent states. Based on this, we also tested some predictions for the whole-cell mI_{CAT} behavior.

MATERIALS AND METHODS

Cell Preparation and Current Recording

Adult male guinea-pigs, weighing 300–400 g, were killed by dislocation of the neck followed by immediate exsanguination according to Schedule one of the UK Animals (Scientific Procedures) Act (1986). Single smooth muscle myocytes from the longitudinal muscle layer of the ileum were obtained after collagenase treatment as previously described (Zholos and Bolton, 1994, 1997).

Whole-cell and single-channel currents were recorded at room temperature using borosilicate patch pipettes of 1–3 and 3–5 MΩ, respectively, and an Axopatch 200B (Axon Instruments, Inc.) voltage-clamp amplifier. For single-channel recordings pipettes were coated with Dow Corning R-6101 elastomer. Current noise was <0.25 pA (rms, 5 kHz bandwidth). Voltage-clamp pulses were generated and data were captured using a Digidata 1322A interfaced to a computer running the pClamp 8 program (Axon Instruments, Inc.). Currents were filtered using the 4-pole low pass Bessel filter of the patch-clamp amplifier at 1 or 2 kHz in whole-cell and single-channel recordings, respectively, and sampled at 48 kHz for storage on a digital tape recorder (DTR-1204; Biologic Science Instruments). In whole-cell experiments series resistance was compensated by 80%. For illustrations, single-channel recordings were digitally filtered (200 Hz lowpass Gaussian filter) and sampled at 500 Hz. Extended portions of the traces that illustrate brief events are shown at the original resolution.

mI_{CAT} was activated by applying carbachol at 50 μM (submaximal concentration, compare with the EC_{50} value of 7.6 μM; Zho-

Published April 26, 2004

los and Bolton, 1997) or by intracellular application of GTPγS at 200 μM by adding it to the pipette solution in order to activate G-proteins directly, bypassing muscarinic receptors.

Solutions and Chemicals

The external solution in which cationic current was recorded consisted of (in mM): CsCl 120, glucose 12, HEPES 10, pH adjusted to 7.4 with CsOH (total Cs^+ 124 mM). Pipettes were filled with the following solution (in mM): CsCl 80, adenosine 5′-triphosphate magnesium salt (ATP) 1, creatine 5, guanosine 5′-triphosphate lithium salt (GTP) 1, D-glucose 5, HEPES 10, BAPTA 10, $CaCl_2$ 4.6 ($[Ca^{2+}]_i$ clamped at 100 nM), pH adjusted to 7.4 with CsOH (total Cs^+ 124 mM). GTP was omitted when guanosine 5′-O-(3-thiotriphosphate) (GTPγS) was added to the pipette solution to activate mI_{CAT} directly. The Cs^+ solutions were used to block currents through potassium channels.

Collagenase (type 1A), adenosine 5′ triphosphate (ATP, magnesium salt), guanosine 5′ triphosphate (GTP, lithium salt), guanosine 5′-O-(3-thiotriphosphate) (GTPγS, tetralithium salt), creatine, N-2-hydroxyethylpiperazine-N′-2-ethanesulphonic acid (HEPES), 1,2-bis(2-aminophenoxy)-ethane-N,N,N′,N′-tetraacetic acid (BAPTA), N-methyl-d-glucamine (NMDG), and carbamylcholine chloride (carbachol) were obtained from Sigma-Aldrich. All other chemicals were from BDH Laboratory Supplies (AnalaR grade).

Data Analyses

Data were analyzed and plotted using pClamp (Axon Instruments, Inc.) and MicroCal Origin software (MicroCal Software, Inc.). For kinetics analyses, the presence of one channel in the membrane patch could be confidently judged since P_O was high (0.43 ± 0.06 in 11 patches selected for kinetics analysis) and no double openings were seen. Quantitatively, the probability of our runs of single openings if there were actually two channels present was estimated according to the equation given by Colquhoun and Hawkes (1995):

$$P(r \geq n_O) = \pi^{n_O - 1}, \quad (1)$$

where $\pi = (1 - P_O)/(1 - P_O/2)$, and n_o is the number of single openings. In the above 11 patches the maximum probability of more than one channel present was of the order 10^{-20}.

Single-channel events were identified on the basis of the half-amplitude threshold-crossing criteria. Transitions <0.16 ms (e.g., rise time for 2 kHz filter, see Fig. 3 A, c) were ignored. This was aimed mainly to ensure consistent time resolution for both openings and shuttings. Imposed resolution in principal makes allowance for missed events but this was not used. Thus, "open" and "closed" intervals were "apparent" intervals.

Histograms of open and closed durations were constructed conventionally as distributions of the logarithm of duration (in ms) (20 bins per decade) with exponential components fitted by the method of maximum likelihood (Colquhoun and Hawkes, 1995). The frequency density and fitted functions were plotted after a square root transformation. The number of probability density function components was determined using the automatic "compare models" routine of the pClamp software at the confidence level of 0.99. Current amplitude histograms were fitted with Gaussian functions. Although four closed states of the channel exist, no burst analysis was done since burst definition would be dubious (e.g., ~10 or more-fold difference in the mean closed times is required).

P_O was determined from idealized traces as the ratio of the sum of all open durations to the total trace duration. All other analysis (correlations, durations of adjacent dwell times, opening frequency analysis, and analysis of channel activity over intervals of certain duration) was done using custom programs.

Cationic conductance activation curves, or P_O values measured at different test potentials, were fitted by the Boltzmann equation in the following form:

$$A = \frac{A_{\max}}{1 + \exp[(V - V_{1/2})/k]}, \quad (2)$$

where A is either cationic conductance (Siemens) or P_O at potential V (volts); $A_{\max}$ is its maximal value; $V_{1/2}$ is the potential at which $A = 0.5A_{\max}$; and k is the slope factor (volts).

For each particular state the probability of being in that state, P_j, was calculated using the following equation:

$$P_j = P_{Class} \cdot \frac{A_j \cdot \tau_j}{\sum_{j=1}^{4} A_j \cdot \tau_j}, \quad (3)$$

where P_{Class} refers either to P_O for open states or to $1 - P_O$ for closed states, A_j is the relative area under the jth exponential component, and τ_j is its time constant (mean dwell time).

Values are given as the means ± SEM; n represents the number of measurements. To determine the statistical significance of differences between the means an ANOVA or a t test were used. Differences were judged to be statistically significant when $P < 0.05$.

RESULTS

General Observations: Three Types of Muscarinic Receptor–gated Cationic Channels in Ileal Myocytes

Under conditions optimal for activation and isolation of whole-cell mI_{CAT} (symmetrical 125 mM Cs^+ solutions, external 50 μM carbachol or internal 0.2 mM GTPγS present) three types of ion channels have been identified in cell-attached (n = 89) and outside-out patches (n = 123) based on the differences in their unitary conductances, kinetics, and voltage dependence. Their ion selectivity properties were not studied in detail (see Inoue et al., 1987; Kang et al., 2001), but it was verified that their unitary currents depended on the Cs^+ ($NMDG^+$ substitution experiments) but not the Cl^- (methanesulfonate substitution) gradient. Also, unitary currents through the three types of channels reversed close to the caesium equilibrium potential, 0 mV. Using Cs^+ as the main charge carrier suppressed currents trough K^+ channels while various TRP channels are similarly permeable to Na^+, K^+, and Cs^+ (for review see Nilius, 2003).

Mean single-channel conductances at potentials around −50 mV were 10.3 ± 0.2 pS (n = 55), 57.1 ± 7.0 pS (n = 52), and 131.8 ± 2.6 pS (n = 51). These three types of cationic channels were identified as channels gated by muscarinic receptor stimulation as Fig. 1 shows. They were also activated by G-proteins since intracellular GTPγS (without agonist application) induced similar channel activation (e.g., Fig. 2).

Fig. 1 A illustrates an example of bath carbachol ap-

Published April 26, 2004

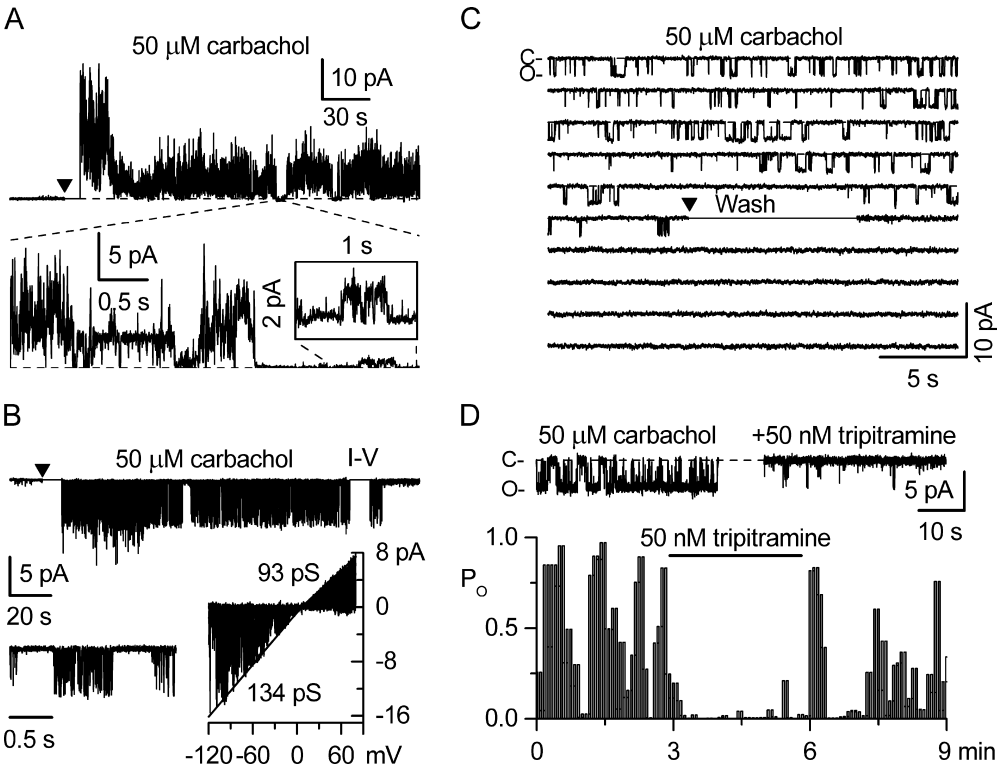

FIGURE 1. Three types of cation channels activated by carbachol application in cell-attached (A) or outside-out (B–D) configurations. Holding potential was 50 mV in A and −50 mV in B–D. Note that current traces were blanked during agonist application in A and B or its withdrawal in C to remove the noise due to the solution exchange that was started at the moment indicated by triangle. Bottom panels in A and B show expanded segments (see dotted lines). Bottom right panel in B shows superimposed 19 leak-corrected traces from the patch obtained by applying 200-ms voltage ramps during the blanked period marked "I-V" in the top trace. Straight lines approximate the maximal current values but most open events were too brief to reach a full open amplitude. (C) An outside-out patch was formed after whole-cell mI_{CAT} was fully activated in response to 50 μM carbachol application; agonist was then removed at the moment indicated by triangle. The traces are consecutive. Channel conductance was 62.8 pS. (D) In another similarly formed membrane patch the M_2-selective antagonist tripitramine was applied at 50 nM for the period indicated by the horizontal bar. The main plot shows P_O values measured in 5-s consecutive intervals, while current traces at the top show examples of channel activity before and after tripitramine application. Channel conductance was 67.2 pS. Horizontal dotted lines indicate closed level.

plication on single-channel activity after a cell-attached patch was formed using 50 μM carbachol-containing patch pipette. As the bottom expanded trace segment in Fig. 1 A shows channel activity consisted of large and frequent but very brief transitions of ~7 pA in maximal size produced by 130-pS channel openings (similar to that shown in Fig. 1 B); longer and hence better defined events of 3.1 pA in size (i.e., 62-pS conductance given the membrane potential of −50 mV) and small openings visible during a few periods of low activity as shown magnified in the inset. The latter were 0.7 pA in size (i.e., 14-pS channel conductance). Fig. 1, C and D, further illustrates that the activity of the 57-pS channel recorded in an outside-out patch (formed after bath 50 μM carbachol application to the whole cell) was terminated upon agonist withdrawal (Fig. 1 C) or could be reversibly inhibited by the M_2-AChR–selective antagonist tripitramine (Fig. 1 D). These observations support the idea that the channel was primarily gated by the M_2 receptor activation (Bolton and Zholos, 1997; Zholos and Bolton, 1997).

In the experiment of Fig. 1 A the 130-pS channel activity lasted 17 min, but it was fairly quickly lost in outside-out patches (on average within 81 ± 19 s, $n = 18$; see top trace in Fig. 1 B showing two channels present initially which cease to open 164 s after carbachol application). This suggests the importance of some freely diffusible second messenger(s). 130-pS channel activity consisted of clear bursts of very brief openings as an expanded trace segment in Fig. 1 B shows, i.e., in this patch at −50 mV mean open times and relative proportions of two fitted exponential components were 0.75 ms (0.69) and 3.53 ms (0.31) resulting in a low P_O, typically <0.1. At positive potentials P_O somewhat increased while single-channel conductance decreased (Fig. 1 B, bottom right), which resulted in average patch current being an almost linear function of voltage.

In contrast, the activity of the 10- and 57-pS channels lasted tens of minutes after patch excision (Figs. 2, 3 A, 9, and 11 A) suggesting that freely diffusible second messengers are not so important for their gating. However, the 57-pS channel could rarely be activated in cell-attached patches (4 in 77) with carbachol in the pipette and/or in the bath (Fig. 1 A), or by carbachol when applied after an outside-out patch was formed (1 in 11).

When a cell-attached patch was formed after cell dialysis with GTPγS (e.g., by using double-patch configuration, or by withdrawing a first patch pipette containing

Published April 26, 2004

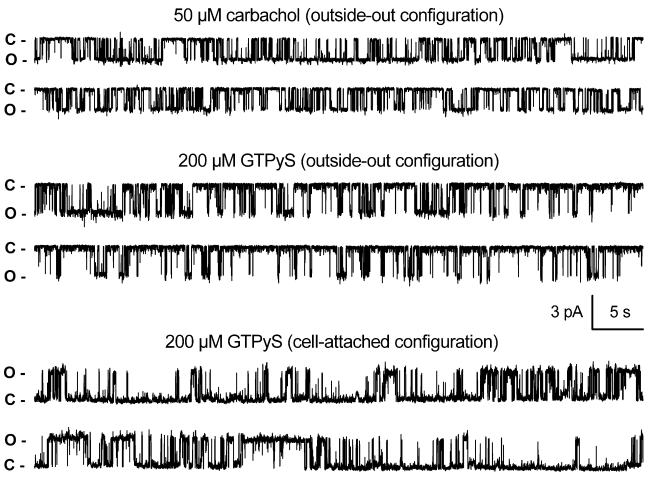

FIGURE 2. Typical examples of muscarinic receptor–gated cationic channel activity recorded in three different outside-out (top and middle) or cell-attached (bottom) membrane patches. The traces in each pair are continuous. Membrane patches were formed by pulling away the pipette after whole-cell mI_{CAT} reached maximum amplitude during the application of either 50 μM carbachol externally or 200 μM GTPγS internally, as indicated. In the latter case if no activity was present in the patch then the same cell was sealed onto using a second pipette filled with the standard external Cs^+-containing solution to obtain cell-attached configuration. Cell-resting potential was assumed to be close to 0 mV since it took at least 3 min for the development of GTPγS-induced current during which time intracellular K^+ would be replaced by Cs^+. The cell was kept in Cs^+ external solution during the whole experiment. In all cases membrane potential across the patch was −40 mV (i.e., 40 mV in the cell-attached configuration). Note that the 10-pS channel activity is present throughout. Closed and open levels in this and subsequent figures are indicated as C and O, respectively.

GTPγS and creating an on-cell patch on the same cell using another pipette) then the 57-pS channel activity was more likely (4 out of 12). A similar proportion was also observed when an outside-out patch was pulled after the whole-cell current had fully developed in response to 50 μM carbachol application (15 out of 50). Thus, it appears that important signaling links need to be established in the whole cell that then remain after patch excision. It is less clear why so few patches with channel activity were obtained in the conventional cell-attached configuration. Kang et al. (2001) noted the same difficulty (2 successful recordings out of 121 trials in their experiments).

In the present work the behavior of the 57-pS channel was analyzed in detail. We have found that this channel has properties that account for the major part of the whole-cell current in the negative range (see below); thus, from the standpoint of the physiological function of the muscarinic cationic conductance this channel type is the most important.

61% of outside-out patches formed after whole-cell mI_{CAT} activation were blank (33 out of 62 in case of GTPγS and 35 out of 50 in case of carbachol stimulation), 19.5% had one (12 out of 62 in case of GTPγS and 10 out of 50 in case of carbachol stimulation), and the remaining 19.5% had multiple active 57-pS channels (from 2 to 7; 17 patches out of 62 in the case of GTPγS and 5 patches out of 50 in the case of carbachol stimulation). In the latter case the probability of seeing 1,2,3. . .N channels simultaneously open followed a binomial distribution closely; thus, the channels gated independently of each other but at the same time they appeared to be clustered in the membrane.

Fig. 2 shows typical examples of single-channel currents activated by carbachol or GTPγS in outside-out and cell-attached patches, as indicated. The membrane potential of outside-out patches was held at −40 mV; the same value was assumed for the cell-attached patch since the holding potential was set at 40 mV and the cell was dialyzed and then kept in a high-Cs^+ solution that would zero its resting potential.

One feature of channel activity was its quite remarkable "mirror" symmetry. For example, although channel openings produce downward deflections in the top and middle pairs of traces and upward deflections in the bottom pair of traces, visually it is hard to tell the difference between them. In other words, channel activity consisted of prolonged bursts of long openings interrupted by brief shuttings, prolonged long closed states interrupted mainly by brief openings, and a series of alternating medium durations opening and closings. Much of the analysis that follows was done to quantify these visual features. Some of this analysis (e.g., P_O change in intervals or sequences of long openings and shuttings) was semiquantitative since a more precise burst analysis would be compromised by a poor separation of the mean closed times (see Table I).

Number of States and Connections Between Them (Markov Chain)

For detailed analyses of channel kinetics we selected one of the longest available records, which is shown in Fig. 3 A, a (326 s; outside-out patch was excised into 50 μM carbachol-containing solution after whole-cell carbachol-evoked mI_{CAT} had fully developed; holding potential was −50 mV). Afterwards, the conclusions were verified and overall mean dwell times and probabilities were calculated by analyzing ten more records in the same manner (mean record duration was 209 s).

In the record shown in Fig. 3, mean P_O was 0.44. Before the channel became unavailable (desensitization at the single-channel level developed abruptly; not depicted) 9,012 transitions occurred, which was sufficient for a rigorous analysis of the channel kinetics. An all-point amplitude histogram (Fig. 3 B) reveals one major peak at −3.12 pA and additional peaks near the baseline level (−0.4 pA) and near the major open level

Published April 26, 2004

TABLE I

Fit Parameters, Relative Probabilities for Each Kinetic State and Estimated Contribution of Each Open State to the Whole-cell Current Amplitude

State	Mean dwell time	Area of component relative to total shut or open time	Relative probability (P_J) of state	Contribution to integral current
	ms			
C1	471 ± 124	0.151 ± 0.023	0.431 ± 0.058	
C2	58.7 ± 12.4	0.229 ± 0.008	0.119 ± 0.023	
C3	4.66 ± 0.75	0.324 ± 0.022	0.015 ± 0.003	
C4	0.66 ± 0.13	0.290 ± 0.021	0.002 ± 0.0004	
O1	0.54 ± 0.10	0.136 ± 0.020	0.0006 ± 0.0001	0.1%
O2	5.43 ± 1.25	0.313 ± 0.023	0.013 ± 0.003	3.0%
O3	46.6 ± 15.6	0.289 ± 0.035	0.104 ± 0.037	24.1%
O4	190 ± 43	0.257 ± 0.034	0.315 ± 0.043	72.8%

Mean values for each state are the average of 11 measurements from outside-out ($n = 9$) and cell-attached ($n = 2$) patches expressing one channel activated either by carbachol ($n = 3$) or by direct G-protein activation with GTPγS ($n = 8$). Mean P_O was 0.432 ± 0.057 ($n = 11$). Mean probabilities of channel being in each of its states (P_J) were calculated using Eq. 3. Contribution of each open state to the whole-cell mI_{CAT} was calculated based on these values. Probabilities and time constants of separate shut and open states were not significantly different for carbachol- and GTPγS-induced channel activities (two-tailed P values ranged from 0.15 to 0.96).

(−3.53 pA) as shown by the dotted lines. Thus, two types of cationic channels are present with conductances of 62 and 8 pS (horizontal bar above the record shows when the latter was particularly active). In fact, there were at least two 8-pS channels in this patch as judged from occasional double openings; the NP_O value was 0.16. This example well illustrates the fact that the 10-pS channel, because of its much lower P_O and unitary current amplitude, makes only a trivial contribution to mI_{CAT} (estimated at 4.84 ± 0.01% [n =12] in the negative range of potentials). Fig. 3 A, b and c, shows short segments of recordings at a higher time resolution. The 190 μs shutting which was just above one rise time (160 μs) is well resolved. The expanded trace in Fig. 3 A, b, also illustrates that typically one or a few brief openings occurred before and immediately after the channel entered a period of gating characterized by long openings and brief closings.

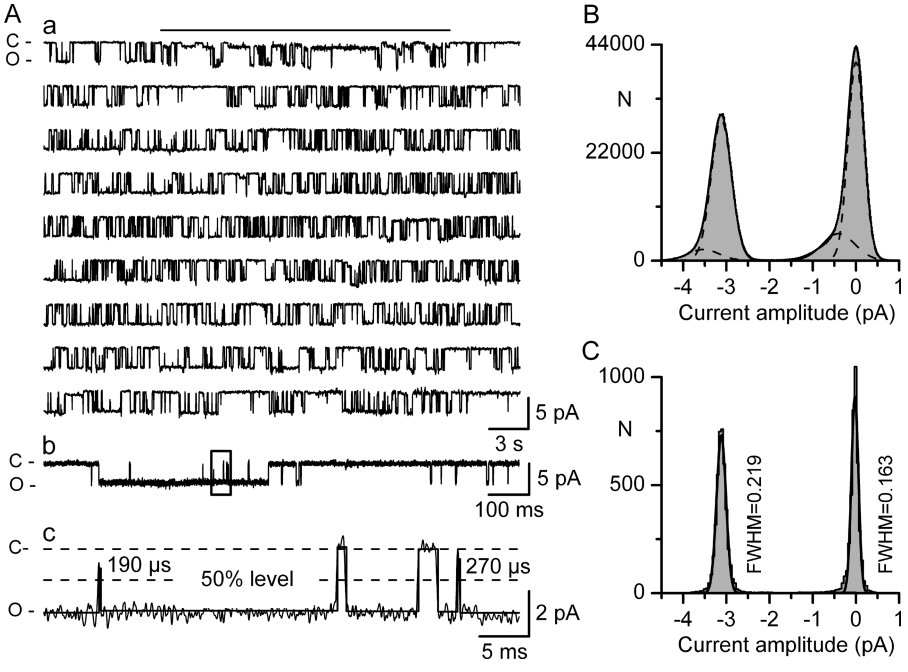

FIGURE 3. Cationic channel activity recorded after patch excision into 50 μM carbachol-containing solution after whole-cell mI_{CAT} had fully developed. (A, a) 326-s continuous recording divided into nine consecutive traces. The horizontal bar indicates a period when the 8-pS channel was particularly active. A, b, shows an extended segment. The box is shown further expanded in A, c (some brief event durations are indicated). Note that the 190-μs closing can be reliably detected. Holding potential was −50 mV. All-point (B) and fitted-levels (C) amplitude histograms were fitted with Gaussian functions (superimposed lines). In the latter case, events shorter than twice the rise time (0.33 ms) were excluded from the amplitude analyses. Note that smaller peaks adjacent to the two major peaks are evident in the all-point amplitude histogram (B); these represent 8-pS channel activity (at least two small conductance channels were present in this patch). Also note, that full width at half-maximum (FWHM) is larger for the distribution of open level amplitudes indicating more current noise when the channel is open.

Published April 26, 2004

Histograms of distributions of apparent closed and open times (20 bins per decade) measured in the experiment of Fig. 3 A are shown in Fig. 4 A. These were fitted with the sum of four exponential components (continuous line, the components are plotted separately). In this and other similar figures mean dwell times and relative areas, which are equivalent to frequency probabilities of being in a particular state, are indicated near each component. Thus, as long as different mean dwell times may be regarded as reporters of different conformations of the channel protein there are at least four open and four closed states of the channel. A model with four open and four closed states will be assumed and used as a basis for further analysis (Scheme I) while accepting that minor contribution by additional states may exist that cannot be detected due to limitations of frequency response of the recording system, and the fitting process/number of acquired events. The scheme is similar to the synergistic model of gating proposed for K_{ACh} channel by Petit-Jacques et al. (1999), whereby ligands interacting with the channel increase its open probability in three stages. The overall structure of cationic channel Markov chain is similar to some other ion channels, such as nAChR (Scheme V given by Colquhoun [1998]), which includes spontaneous channel openings in the absence of agonist), BK_{Ca} channel (Scheme II given by Cox et al. [1997]), or hyperpolarization-activated HCN channel (Altomare et al., 2001).

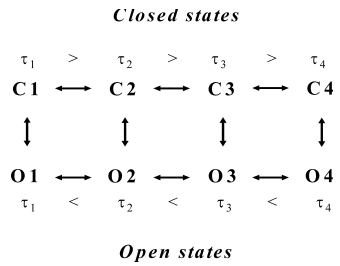

SCHEME I

To reveal adjacent states in the model (Scheme I) durations of adjacent closed and open states were measured. Qualitatively, the plot of open intervals versus adjacent shut time in Fig. 4 B shows that with very few exceptions (6 out of 4,506) there is a strong inverse relationship between the duration of openings related to closed events. This is true for both next and previous open durations as illustrated in the insets. Quantitatively, these correlations were evaluated by measuring mean time of open events adjacent to closed durations in four ranges that corresponded to the time constants of four components of the closed time distribution (indicated by triangles in Fig. 5, the chosen range was ±5 bins around the corresponding mean closed time) as suggested by McManus et al. (1985). The differences between mean open times were statistically significant (note that different symbols show data calculated separately for previous, next and both adjacent open intervals). The histogram shown by the dotted line illus-

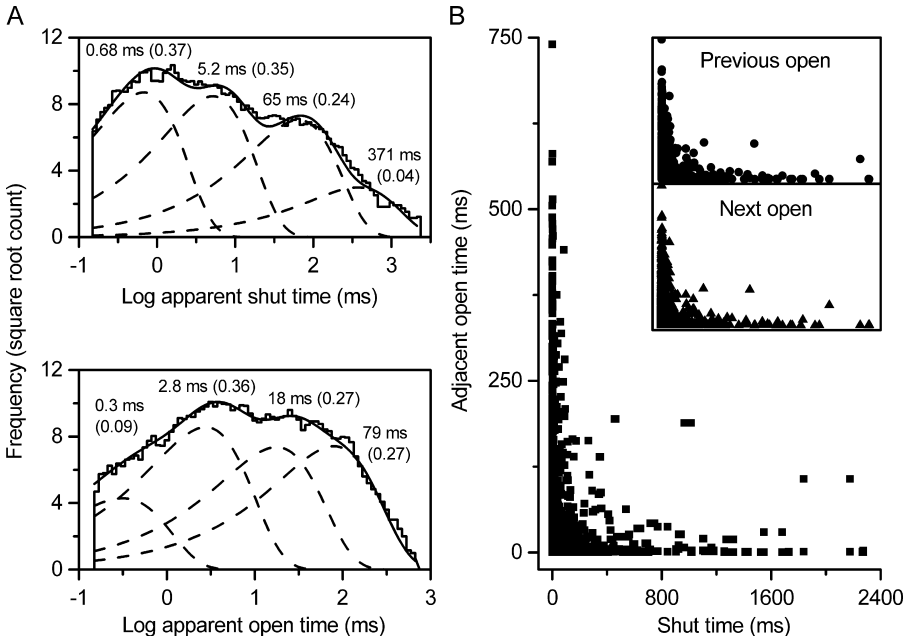

FIGURE 4. Kinetics states of the cationic channel and correlations between adjacent intervals. (A) Histograms of distributions of apparent closed and open durations measured in the experiment illustrated in Fig. 3 A. 20 bins per decade was used in this and similar subsequent figures. Note that frequency is shown conventionally on the square root scale. The histograms were fitted with exponential components by the maximum likelihood method as shown by the continuous line. Exponential components are shown with mean dwell times and relative areas (in parentheses) indicated. Raw data were fitted but adjacent two-point smoothing was used to produce the final plots of the histograms to allow a better visualization. (B) Relationship between adjacent event durations. Data points for all adjacent open durations (previous and next openings related to a closing) are shown in the main plot, while the insets illustrate these relationships separately for previous and next open durations plotted against closed event duration. Only six points are not clustered near the zero coordinates.

Published April 26, 2004

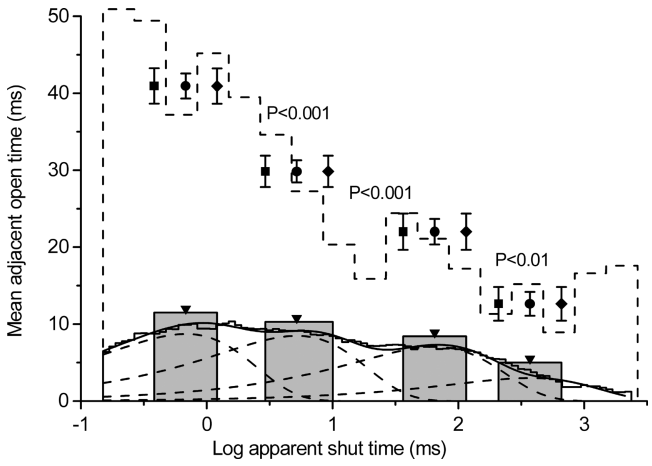

FIGURE 5. Analyses of adjacent intervals. Histogram of distribution of closed durations is shown at the bottom for comparison (same as in Fig. 4 A, top) with the four ranges used for analysis indicated by the gray columns. Each range was centered (±5 bins) around a mean closed time (triangles). Thus, for $\tau_1 = 0.68$ ms the range was 0.382–1.21 ms; for $\tau_2 = 5.19$ ms: 2.92–9.23 ms; for $\tau_3 = 64.8$ ms: 36.4–115.2 ms; and for $\tau_4 = 371$ ms: 209–660 ms. The mean durations of previous (squares), next (diamonds), and both (circles) open intervals are plotted for each range. Since the intervals do not follow normal distribution, for assessment of the statistical significance of the differences a Kruskal-Wallis test (nonparametric ANOVA) was used which gave $P < 0.0001$. Dunn's multiple comparisons test gave the P values as indicated. Dotted-line histogram shows the same relation over the whole range using groups of five bins.

trates the correlations over the entire range, without any assumption as to the number of channel states.

It follows from the correlation analysis that the connectivity (Colquhoun and Hawkes, 1995) of open and shut states was greater than unity, which imposes a restriction on the Markov chain such that no single state should exist that, if deleted, will separate the open states from the shut states (see more about the origin of correlations in Colquhoun and Hawkes, 1995).

The possibility was considered that patch excision might have altered channel gating, for example due to cytoskeleton deformation or disruption as already mentioned in connection with difficulties of activating the channel in certain patch-clamp configurations. Alternatively, such alterations could arise due to the loss of some important diffusible cellular second messengers. Thus, control experiments were performed where mI_{CAT} was activated by intracellular application of GTPγS (see Fig. 13 A as an example) and as soon as mI_{CAT} reached a peak amplitude the patch pipette was removed and an on-cell patch was formed using a second pipette filled with the standard Cs^+ external solution. Since GTPγS activates G-proteins almost irreversibly, channel activity could be recorded in the cell-attached configuration even though the agonist was absent.

Fig. 6 shows the results of the analyses of channel activity recorded under these conditions (original trace segments obtained from this patch were shown in Fig. 2, bottom pair). Channel conductance was 59 pS as estimated from the unitary current amplitude of 2.36 pA at a holding potential of 40 mV (membrane potential −40 mV). 13,861 events observed during 775 s were subject to the same analysis as described above. Exponential components in open and closed time distributions as well as their relative areas were very similar to those observed for the carbachol-gated channel in an outside-out patch (compare Figs. 6 A and 4 A; statistical tests presented in the Table I legend). An important conclusion that follows from this observation is: although channel P_O is increased through its interaction with the Gαo-GTP molecule (Yan et al., 2003), likely by increasing the probability of transition toward the O4 state (see below) the channel possesses an intrinsic gating mechanism that kinetically remains the same whether Gαo is bound to the hydrolyzable GTP or to the much more stable GTPγS (compare with similar observations in case of K_{ACh} channel by Ivanova-Nikolova and Breitwieser, 1997). In other words, bursts of long openings that account for the major part of mI_{CAT} (see below), and hence likely arise due to the interaction with activated Gαo-GTP, are not terminated simply because GTP is hydrolyzed and inactive Gαo-GDP is formed.

Correlation analysis of adjacent closed and open states also produced a similar result (compare Figs. 6 B and 4 B). We did not calculate the dependence of mean adjacent open intervals over selected ranges of closed times as in Fig. 5 (symbols), since compiling the histogram over the whole range was more straightforward. These are shown in Fig. 6 C by columns for this patch and by circles for the average data from 11 patches. Maximum open time in each patch was normalized as 1.0 irrespective of where the maximum occurred (e.g., the second column in the histogram of Fig. 6 C). Absolute maximal values in different patches varied from 45 to 260 ms with a mean of 109 ± 23 ms ($n = 11$).

From these results we conclude that the states are connected as shown in Scheme I (mean values from 11 patches are shown in Table I).

Cycling Behavior within Markov Chain of Cationic Channel

Many novel features of K_{ACh} channel in heart, such as four distinct modes of gating of the G-protein–gated K_{ACh} channel, were revealed by analysis of its P_O and the frequency of openings after dividing a continuous record into consecutive segments of fixed duration (Ivanova-Nikolova et al., 1998). Thus, we have performed a similar analysis. Some of our results are consistent with the above study, but novel features were

Published April 26, 2004

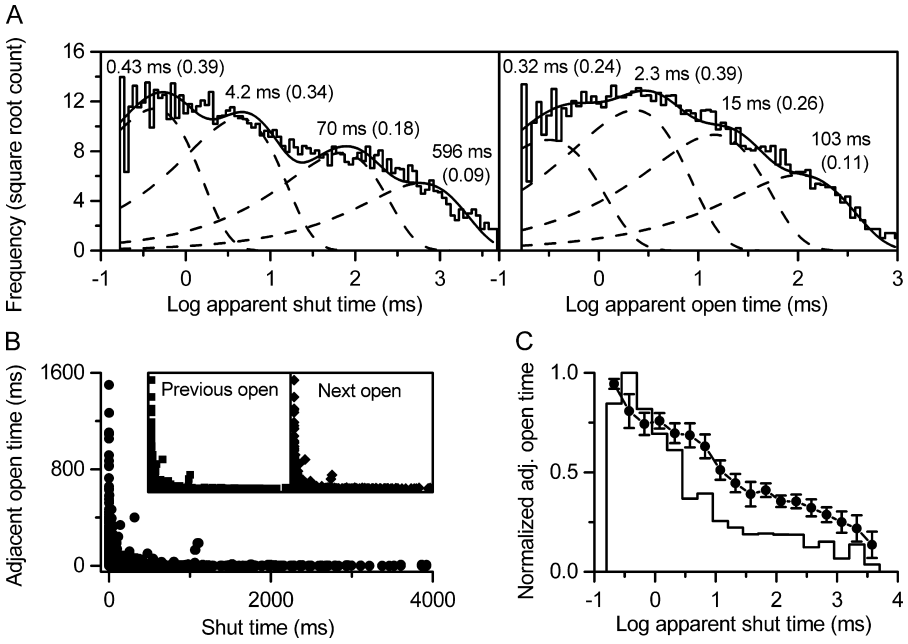

FIGURE 6. Analysis of cationic channel activity that was induced by direct activation of G-proteins using GTPγS and recorded in the cell-attached configuration (see Fig. 2, two traces at the bottom). (A) Histograms of distributions of apparent closed and open durations. (B and C, histogram) Correlation analysis performed as in Figs. 4 B and 5, respectively. Circles in C show mean data (±SEM) from 11 observations.

also found. Notably, while it was found that the K_{ACh} channel P_O increases from mode 1 to mode 4 mainly because the channel opens progressively more frequently and for longer durations, cationic channel P_O is mostly determined by cycles within the Markov chain (e.g., the number of long open states, O_L, encountered before it enters a long shut state, C_L).

Fig. 7 shows P_O measured over 5-s intervals from the record in Fig. 3 A. Mean frequency of channel openings was 13.8 s^{-1}, thus on average 69 openings were included in each interval yet there was a significant scatter of P_O values in the range of 0.005–0.89. Since the O4 state generates 73% of the integral current (Table I) its frequent occurrence could explain periods when P_O was high while frequent occurrence of the C1 state might explain periods when P_O was very low. All occurrences of C1 and O4 states given the overlapping distributions are not possible to quantify but a phenomenon known as length-biased sampling is known (Colquhoun and Hawkes, 1995). This arises due to a positive skew of the exponential distribution; as a result above-average dwell times are fewer in number but make a greater functional contribution. Thus, we restricted our analysis to include only O_L and C_L states defined, respectively, as openings >79 ms and closings longer than 371 ms (based on distributions of Fig. 4 A). These are plotted at the top of Fig. 7. Their total contribution to the trace duration amounted to 24.3% for the C_L state and 33.6% for the O_L state. Considering the areas under exponential components, it can be calculated that 95.2% of C_L belong to the C1 state and 97.1% of O_L belong to the O4 state. Although such definitions include only 37% of C1 and O4 states because of the above-mentioned phenomenon C_L and O_L account for 74% of the total time occupied by C1 and O4 states, respectively.

It was also found, as with the K_{ACh} channel, that the frequency of openings increased as P_O increased (correlation coefficient $R = 0.59$; $P < 0.0001$). Thus, there is a possibility that several frequency modes exist for the cationic channel, but they are not as distinct as for the K_{ACh} channel (Ivanova-Nikolova et al., 1998). In contrast, as shown in Fig. 8 A (squares) there was a close relationship between P_O measured in 5 s sequential intervals and the number of visits to the O_L state between consecutive visits to the C_L state in the same intervals. The number varied from 0 (e.g., two C_L states with no O_L in between) to a maximum of 45 (i.e., 45 openings >79 ms occurred before a closing longer than 371 ms; 39 was the average value). The mean value of the number of O_L openings after one C_L was 5.5 ± 0.9 ($n = 99$).

The number of visits to the C_L state between consecutive O_L was much smaller, ranging from 0 to 5 with the average of 0.18 ± 0.02 ($n = 546$) (Fig. 8 A, circles). However, in this patch mean P_O was high and thus one could expect a converse at low mean P_O in which case the number of visits to C_L state between consecutive visits to O_L state could become an important factor in determining P_O (see below).

The mean open and closed times were also measured over the same 5-s intervals and these values are plotted against P_O in Fig. 8 C, which further revealed that a decrease in the mean closed time (closed circles) makes a more significant contribution. Finally, the histogram of P_O measured in 5-s consecutive intervals (Fig. 8 B) revealed that (using the same terminology as for the K_{ACh}

Published April 26, 2004

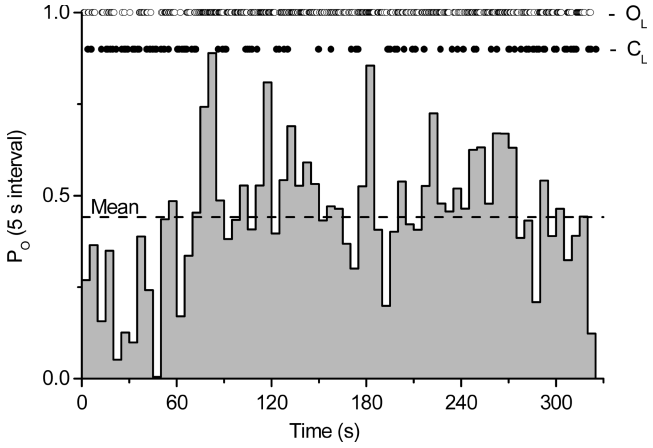

FIGURE 7. P_O values measured over 5-s consecutive intervals from the record in Fig. 3 A. The horizontal dashed line indicates the mean P_O value. The occurrence of C_L (>371 ms) and O_L (>79 ms) states is indicated at the top.

channel) modal preferences of gating of the cationic channel exist that are not so much in the frequency domain but rather in the open probability domain (which in turn is related to the number of O_L states between consecutive C_L states). Thus, three modes of P_O can be visualized with mean values and areas under Gaussian curves of 0.14 (16%), 0.45 (70%), and 0.72 (14%) (Fig. 8 B). This graph shows that channel gating is highly heterogeneous even if the trace is arbitrarily divided into consecutive 5-s segments (as mentioned, these include on average 69 openings in each interval). According to the mean parameters in Table I four modes should exist with characteristic P_O values of 0.001, 0.085, 0.909, and 0.996 and fractional times of 0.43, 0.13, 0.12, and 0.32, respectively. However, these are not seen in Fig. 8 B because the channel changes its gating mode frequently (as evident from the occurrences of O_L and C_L in Fig. 7) and dividing the trace in a mode-specific segments has the same problem as burst analysis namely that channel state cannot be unequivocally identified from burst events (see MATERIALS AND METHODS).

It is interesting to note that if P_O was measured over shorter intervals (e.g., 400 ms as for K_{ACh} channel) then two major peaks at $P_O = 0.03$ and $P_O = 0.98$ appeared while the peak at $P_O = 0.45$ disappeared, suggesting a better discrimination between the modes. Constructing a moving average of these data points by symmetrical averaging of 15 adjacent points revealed a striking cycling behavior with a rather constant period between

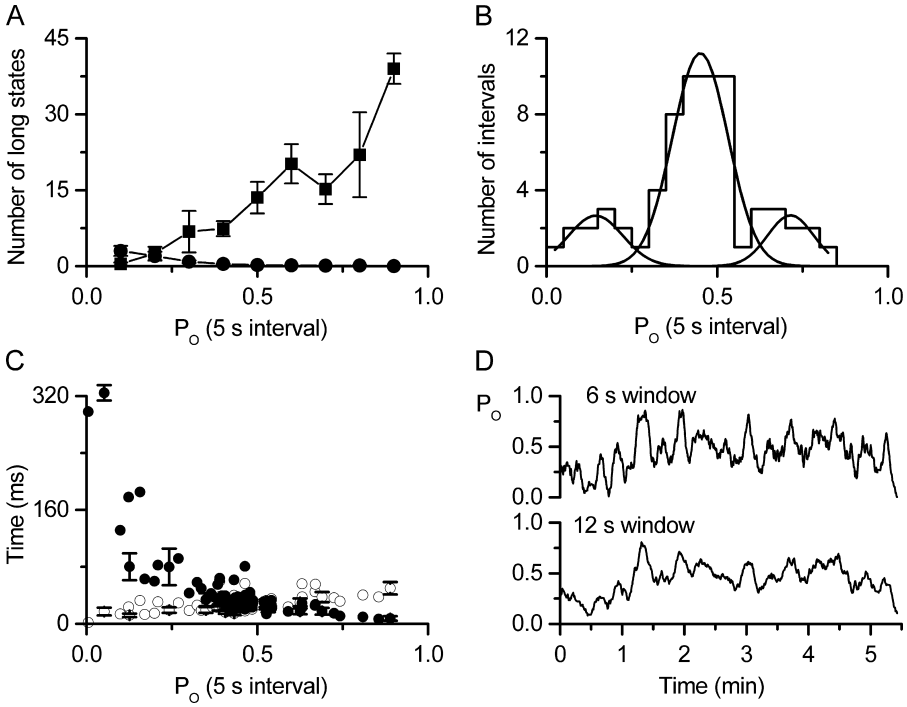

FIGURE 8. The number of visits to the O_L state that occur between visits to the C_L state is the major determinant of P_O and cycling behavior of cationic channel activity. (A) The relationship between this number (squares) and P_O measured in 5-s consecutive intervals. In each 5-s segment the average number was formed from: (a) the number of O_L states which followed each C_L state (if any) in that segment; (b) the number of O_L states that followed the last C_L state in the previous segment(s) before the first C_L state in that segment; and (c) the number of O_L states that followed the last C_L state in that segment before first C_L in the next segment(s). The average number of visits to the C_L state that occur between visits to the O_L state calculated by the same algorithm is also shown (circles). (B) Histogram of P_O values measured in 5-s consecutive intervals fitted by three Gaussian components (the mean values and areas are indicated in the text). (C) Averaged open (open circles) and closed (closed circles) event durations measured in each 5-s segment plotted against P_O of the same segment. (D) Regular cycles of P_O change during the experiment (see text for more details). We verified that averaging data points over a moving window of twice the size did not change the number or position of these apparent P_O peaks (compare top and bottom traces). Note, that we used symmetrical averaging that does not produce a time shift and that the moving average filter, due to its very slow roll-off, has little ability to separate one band of frequencies from another (Smith, 1997). Note that the same result can be obtained by measuring P_O in a 6-s window sliding with a 400-ms increment. Also note that at lower mean P_O, mixed gating produced less scatter of data points in 5-s segments and hence similar oscillations could be visualized more directly in raw data (see Fig. 9 B).

Published April 26, 2004

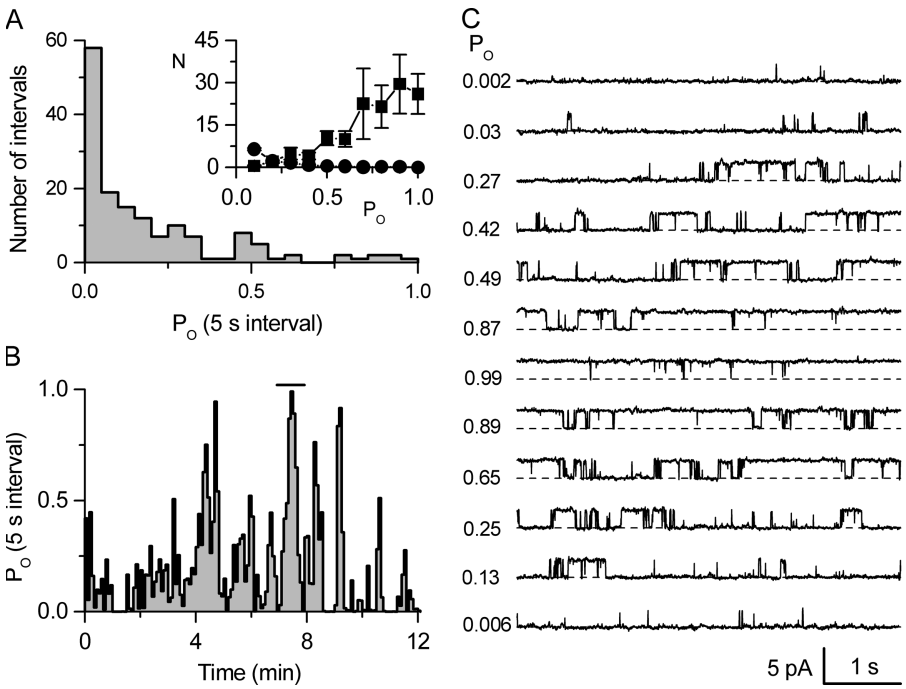

FIGURE 9. Cycling behavior of P_O in a cell-attached patch. In A and B the analysis was similar to that described in Figs. 8 B and 7, respectively, for a patch with gating kinetics analyzed in Fig. 6 A; hence, the long states were defined as follows: $O_L > 103$ ms and $C_L > 596$ ms. Considering the overlap between exponential components, in this example 99.9% of C_L belong to the C1 state and 99.6% of O_L belong to the O4 state. The inset in A shows results of the analysis similar to that in Fig. 8 A and on the same scale. Squares and circles show the mean number of consecutive O_L and C_L states, respectively. (C) Consecutive 5-s segments recorded during the period indicated by the horizontal bar in B, which corresponds to one complete cycle of P_O. Note that P_O values of ~0.5 result from mixed gating (compare with the major peak in Fig. 8 B), whereas periods of very low and very high P_O clearly result from gating in, respectively, C1-O1 and C4-O4 pairs of states according to Scheme I. The dotted line shows the closed level.

the peaks of ~20 s (Fig. 8 D, top trace). It can be noted that the moving average filter is optimal for random noise reduction (e.g., by a factor of $15^{1/2}$ in Fig. 8 D; top trace) while keeping the sharpest step response and thus is ideal for analyzing signals in the time but not in the frequency domain (Smith, 1997). Two observations suggested that the oscillations of P_O were not a data filtering artifact. First, averaging P_O over a window of twice the size did not noticeably reduce their frequency (bottom trace in Fig. 8 D). Second, in some patches, particularly when the channel had a lower mean P_O, the cycling behavior could be visualized in the raw data (e.g., Fig. 9 B). Peaks of P_O arise from runs of long openings (see Fig. 8 A and Fig. 9 A, inset) that could be related to periodic channel interaction with Gαo-GTP (or, less likely, other ligands), but this hypothesis needs further tests.

Similar analysis was done for a cell-attached patch as shown in Fig. 9, A and B. In this patch channel mean P_O was much lower (0.18) and the histogram of a number of 5-s intervals versus P_O revealed one expected major peak at $P_O < 0.05$ (Fig. 9 A). The number of O_L states between consecutive C_L states ranged from 0 to 40 while runs of C_L between consecutive O_L states ranged in number from 0 to 14. Somewhat surprisingly, their overall dependence on P_O was the same as in the patch with a higher P_O (compare insets in Figs. 9 A and 8 A). It can be concluded that, despite a considerable difference in overall P_O, periods with similar P_O are characterized by a similar number of consecutive O_L or C_L states. Thus, the major factor that determines a higher overall P_O appears to be a high frequency of periods of high P_O (compare histograms in Figs. 9 A and 8 B).

Plotting P_O measured in consecutive 5-s intervals versus time revealed even better defined oscillations (Fig. 9 B, note that raw data are plotted, i.e., no moving average was used). Analysis of all 11 patches studied showed that the period between peaks of P_O well correlated with the mean P_O value which ranged from 0.18 to 0.78 ($R = -0.9$; $P = 0.0002$).

Fig. 9 C illustrates a complete sequence of changes in channel gating kinetics during a single P_O oscillation indicated by the horizontal bar in Fig. 9 B (i.e., continuous 60-s record divided into 5-s segments). Clearly, the channel starts gating in the C1-O1 pair of states (two top traces), then periods of long openings with associated brief shuttings appear resulting in a gradual P_O rise in Fig. 9 B (e.g., mixed gating in several modes during one segment). Finally, the channel enters an ~15-s long period of C4-O4 gating resulting in a P_O value close to 1.

In conclusion, activity of this channel at constant stimulation is heterogeneous because of alternating periods of low and high P_O such that its mean P_O is encoded by the frequency of P_O oscillations. Equating O_L with the O4 state, and the C_L with the C1 state, will produce under- and overestimates, respectively, of the true number of O4 and C1 states; the net effect on the results may be not too different from the values shown.

Published April 26, 2004

The Origin of Voltage Dependence of mI_{CAT}

The whole-cell current displays a distinctive I-V relationship that is prominently U-shaped at negative potentials, whereas around the reversal potential there is another characteristic region of double rectification (Fig. 13 B). At the time this was discovered this seemed a unique property of mI_{CAT} (Benham et al., 1985), but now it is recognized as a common property of cationic channels formed by TRP proteins, particularly in the case of TRPC3 to TRPC7 (for review see Clapham, 2003). As was already mentioned, it is likely that the muscarinic cationic channel also belongs to this group. The origin of this complex I-V relationship is not so clear. Previous studies have established that the voltage dependence of P_O explains the U-shaped I-V relationship in the negative potential range, whereas around 0 mV and at more positive potentials channel openings and closings could not be resolved even in the absence of intracellular Mg^{2+} or polyamines (Inoue et al., 1987; Kang et al., 2001). Thus, the aim of the next series of experiments was to discover which changes in channel kinetics are responsible for the voltage dependence of P_O, and through this to find out which transitions in the underlying Markov chain are sensitive to membrane potential.

Fig. 10 A shows an example of open and closed times histograms obtained by observing cationic channel activity in an outside-out patch which was exposed to carbachol and recorded either at −40 mV (408 s, mean $P_O = 0.59$) or at −80 mV (334 s, mean $P_O = 0.34$). Fitting exponential components revealed that the decrease of P_O evoked by membrane hyperpolarization was associated with changes of the mean dwell times (particularly in the case of C1 and C2 states), but at the same time there was only a small net redistribution between the states, i.e., relative areas of the components changed little.

Channel activity over a wide range of test potentials was investigated using an outside-out patch formed after whole-cell mI_{CAT} was fully activated in response to intracellular application of GTPγS (see examples in Fig. 11 A). Analysis of exponential components of closed and open time distributions revealed that the time constants showed voltage dependence while the relative areas (e.g., probability of being in one of eight closed or open states) were little affected; the latter showed some scatter but there was no particular voltage-dependent trend (Fig. 10 B, bottom).

It can be seen that membrane depolarization increases both the frequency of openings and their durations (Fig. 11 A). If a step from −50 to 30 mV was applied then channel flicker developed instantaneously but this was lost when the membrane potential was stepped back to −50 mV. A trace at the bottom shows this flicker behavior at a higher resolution. Individual

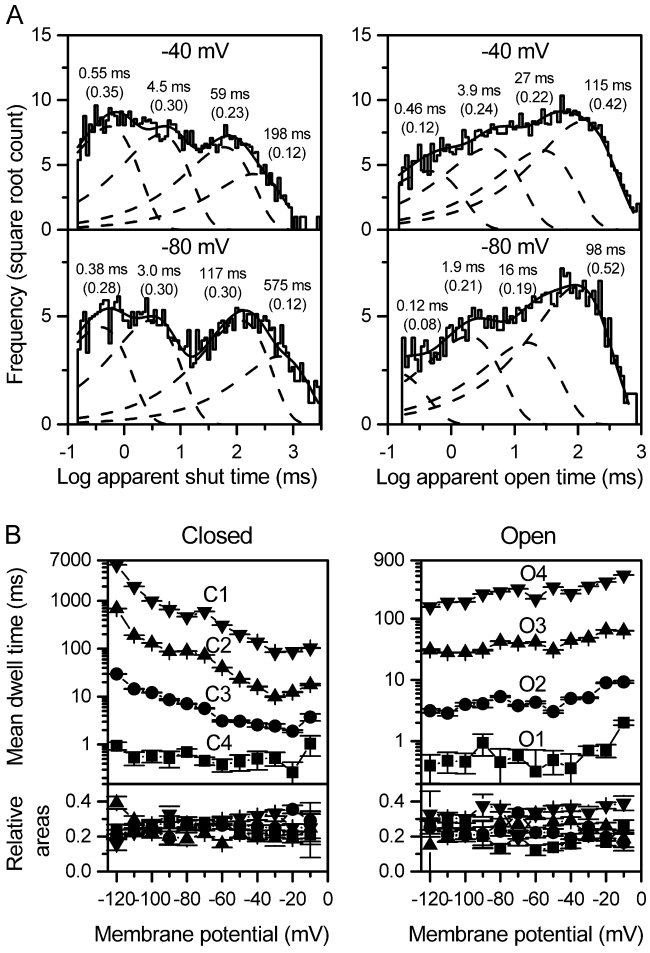

FIGURE 10. The effect of membrane potential on channel gating. (A) Histograms of distributions of closed and open durations measured in an outside-out patch exposed to 50 μM carbachol and held at two potentials as indicated. Note that depending on the membrane potential the time constants change but the relative areas remain much the same. (B) Parameters of the exponential components of closed (left) and open (right) time distributions plotted against test potential for the GTPγS-induced channel activity illustrated in Fig. 11 A. Different symbols in the bottom panels refer to the states denoted in the top panels by the same symbols. The relative areas of each closed or open state are plotted. The states are numbered according to Scheme I. At −40 mV, 7,582 events in 408 s. At 280 mV, 3,260 events in 334 s.

openings and closings could not be resolved, in fact even the baseline current level was hard to determine as the channel spent most of the time in the open state, which was extremely noisy and of much reduced amplitude because of high frequency partially resolved closings. Thus, analysis of channel kinetics was restricted to potentials negative to 0 mV.

Unitary and mean patch currents are plotted versus test potential in Fig. 11 B (squares and circles, respectively). These I-V relationships are similar to, respectively, instantaneous and steady-state I-V relationships

Published April 26, 2004

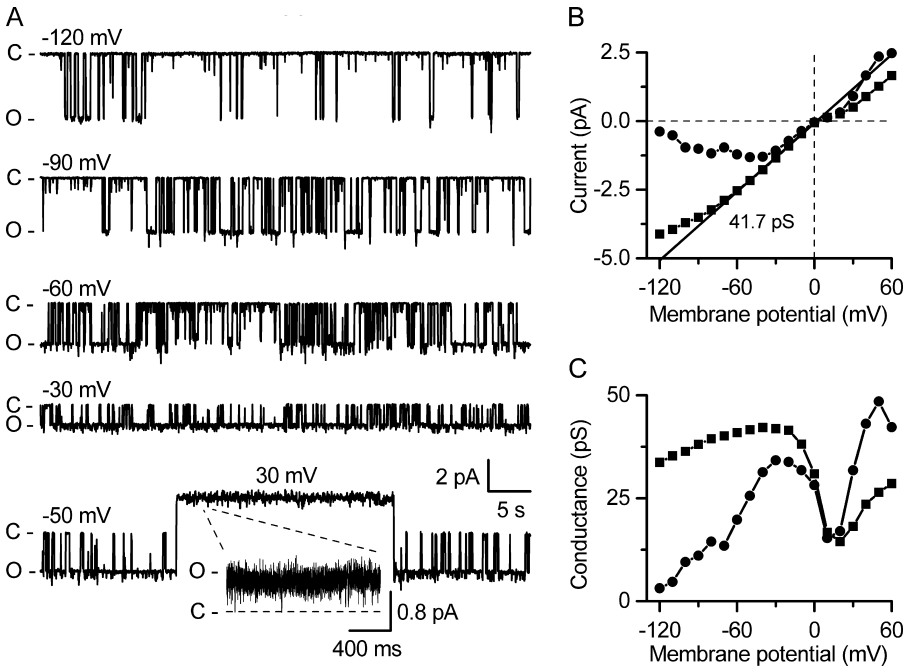

FIGURE 11. Voltage dependence of cationic channel gating. (A) Channel activity at different test potentials was measured in an outside-out patch formed after whole-cell mI_{CAT} was fully activated in response to intracellular application of GTPγS. Bottom trace shows instantaneous development of flicker block of the channel upon a voltage step from −50 to 30 mV. The block was instantly removed after the holding potential was returned to −50 mV. (B) Voltage dependence of single-channel current (squares) and mean patch current (i.e., current integral which measures the transferred charge Q divided by the trace duration t, so that mean $I = Q/t$ as shown by circles). Note that a 9-pS channel is also present in this patch but makes a negligible contribution to the mean patch current at negative potentials, but at 60 mV its contribution was estimated to be ~20%. (C) Single-channel conductance (squares) and activation curve (circles) determined by dividing corresponding current amplitudes in B by the driving force ($V - V_{rev}$) at each potential, where V_{rev} is the reversal potential. Activation curve data points could be fitted by Eq. 2 with a potential of half-maximal activation of −58.0 mV and a slope factor of −22.9 mV; these parameters were similar to those describing P_O voltage dependence (see Fig. 12 A).

of the whole-cell mI_{CAT} (Benham et al., 1985; Inoue and Isenberg, 1990b; Fig. 13 B). Corresponding conductance curves denoted by the same symbols are shown in Fig. 11 C. These show that the major factor that accounts for the decrease of mI_{CAT} conductance in the range 0–30 mV is an apparent reduction of both unitary current amplitude and P_O as a result of very short but frequent shuttings (Figs. 11 A and 12 A). The combined effect produces an overall N-shaped cationic conductance curve (Fig. 11 C, circles) that is similar to the whole-cell activation curve (Fig. 13 C).

Fig. 12 A shows the voltage dependence of P_O described by the Boltzmann function (Eq. 2) with the parameters indicated. Open symbols indicate the values that were estimated from all-points amplitude histograms since a channel event search algorithm could not be used in the presence of channel flicker block. Thus, at positive potentials unitary amplitudes (Fig. 11 B) and P_O values (Fig. 12 A) were evaluated from, respectively, peaks and areas of two overlapping Gaussian curves fitted to all-points amplitude histograms. Mean parameters describing the voltage dependence of P_O were as follows: P_O maximal value 0.81 ± 0.09, potential of half-maximal activation −83.9 ± 10.7 mV and slope factor −19.9 ± 4.0 mV (n = 4). Whole-cell cationic conductance was also examined just before patch formation by applying a slow 6 s voltage ramp from 80 to −120 mV. Corresponding parameters were −89.0 ± 7.2 mV for the $V_{1/2}$ value and −19.0 ± 1.5 mV for the slope. Paired t test (two-tail) showed no difference between single-channel and whole-cell current voltage dependence ($P = 0.24$ in case of the $V_{1/2}$ value and $P = 0.81$ in case of the slope factor; $n = 4$). Moreover, when the $V_{1/2}$ values were analyzed there was significant correlation ($P < 0.001$) between single channel and whole-cell data. This was absent for the slope factor ($P = 0.34$).

These values were also within their typical range as found in a larger population of cells in which only whole-cell parameters were examined. Thus, during the steady-state response to 50 μM carbachol the $V_{1/2}$ value was −98.8 ± 3.2 mV (ranged from −57 to −137 mV; n = 39) and −83.1 ± 1.4 mV in case of GTPγS-induced current (ranged from −63 to −105 mV; n = 48).

Two factors that determined the change in P_O when membrane potential was changed were an increase of the mean open time as well as a parallel decrease of the mean closed time (Fig. 12, B and C). For both mean dwell times there was an e-fold change per ~24 mV, similar to the slope factor of the P_O voltage dependence.

An important conclusion emerges from this analysis. In the Markov chain of the cationic channel shown in Scheme I all the vertical transitions between adjacent closed and open states are voltage dependent, but there is little horizontal redistribution between the states when membrane potential is changed. Thus, horizontal transitions are likely to be governed by ligands

Published April 26, 2004

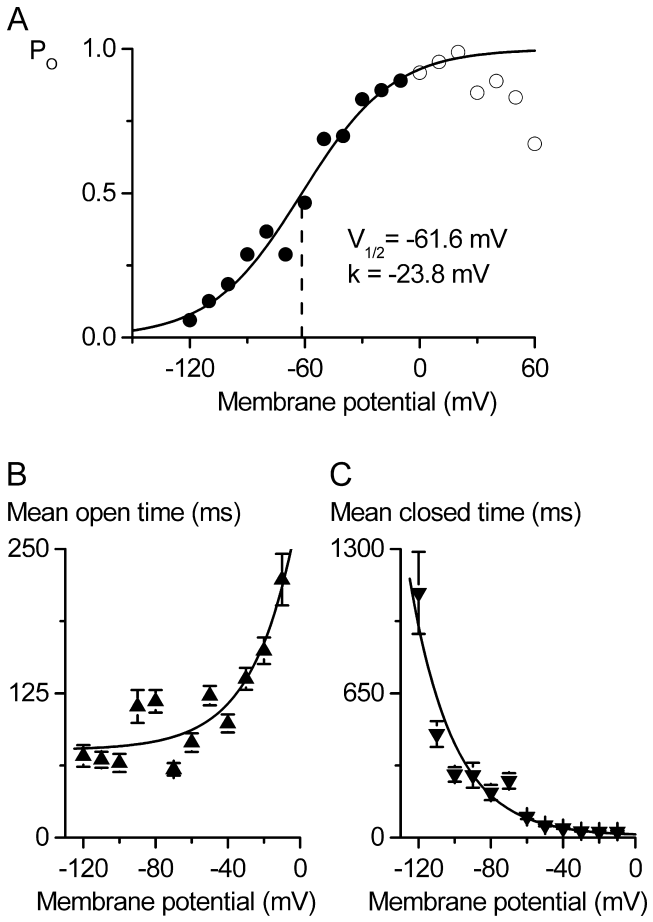

FIGURE 12. Voltage dependence of single-channel behavior. (A) Voltage dependence of P_O. Data points at negative potentials were calculated as described in MATERIALS AND METHODS. The values shown by open circles were estimated as relative areas after fitting all-points amplitude histograms with Gaussian curves. (B and C) Mean open and mean closed times, respectively, plotted against test potential. The data points were approximated by single exponential functions as shown by the smooth lines. Note that between −120 and −10 mV the mean closed time decreases 40-fold compared with a moderate threefold increase of the mean open time.

that interact to open this channel (see DISCUSSION) and these ligands need not interact with the channel in a voltage-dependent manner.

Markov Chain Predictions for the Whole-cell Current Behavior

A system with states and connections as shown in Scheme I has a substantial potential for shifting behavior. This was previously analyzed in detail for the BK_{Ca} channel that has 10 main "condensed" states (Scheme II of Cox et al., 1997). An important analogy is that vertical transitions are voltage dependent, whereas horizontal transitions are ligand but not voltage dependent. Although ligands are different with regard to the mechanisms of their interactions with the channel, in both cases P_O is increasing when the gating shifts from left to right simply because more heavily contributing O2, O3, and O4 states generate progressively longer openings. Thus, a roughly parallel negative shift of the activation curve is to be expected according to the formalism of Eq. 4a given by Cox et al. (1997) for BK_{Ca} channel:

$$P_O = \frac{1}{1 + B \cdot L(0) \cdot \exp(-QFV/RT)}, \quad (4)$$

where B depends on $[Ca^{2+}]_i$ and all the Ca^{2+} dissociation constants for both the closed and open channel, L(0) is the open-to-closed equilibrium constant in the absence of Ca^{2+} at 0 mV, Q is the equivalent channel gating charge, F is Faraday's constant, V is membrane potential, R is the universal gas constant, and T is the absolute temperature. In the absence of calcium (i.e., B = 1) parameter L(0) thus determines the $V_{1/2}$ value due to intrinsic voltage dependence of the channel, but in the presence of channel ligand (B < 1) the curve shifts negatively.

Fig. 13 A illustrates one of our standard whole-cell experiments designed to activate cationic channels directly by intracellular application of GTPγS, which was usually followed by patch excision after mI_{CAT} reached a maximum. In this experiment, however, slow voltage ramps were applied at 20-s intervals starting immediately after break-through (Fig. 13 A, triangle). As can be seen in Fig. 13 B, pronounced changes of the shape of the I-V curve accompanied current development. These were translated into conductance curves plotted in Fig. 13 C and fitted by the Boltzmann function (Eq. 2) in the range −120 mV to about −40 mV. Superimposed fitted functions were extended to 80 mV, which allowed evaluation of the effect of the flicker block of the channel described above but only the unblocked part of each trace was included in the fit range. There was, as expected, a roughly parallel negative shift of the activation curve during the time course of mI_{CAT} development that, in turn, was presumably due to the accumulation of GTPγS-bound α subunits of G-proteins (note that GTP was not added to the pipette solution when GTPγS was used). A similar phenomenon exists when carbachol concentration is increased but the opposite shift is seen during desensitization in the absence of GTP (Zholos and Bolton, 1994, 1996). For 13 fitted traces the slope factor was −19.7 ± 1.7 mV, very close to the value of −19.9 ± 4.0 mV (n = 4) describing the slope of P_O voltage dependence (Fig. 12 A). The $V_{1/2}$ value shifted ~40 mV in the negative direction simultaneously with the increase of the maximal conductance (Fig. 13 D). It can be noted that in this example the $V_{1/2}$ shifted negatively by ~20 mV more compared with the typical value of −83 mV but the starting value was also somewhat negative.

A fit of the same quality could be obtained using an

Published April 26, 2004

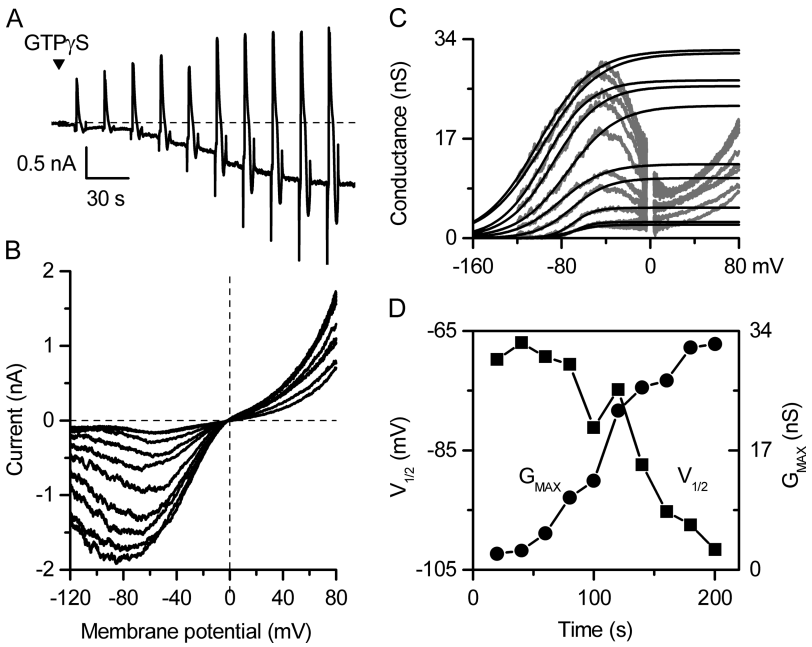

FIGURE 13. Change of the steady-state voltage dependence of the whole-cell current during gradual G-protein activation by GTPγS. (A) A typical current recording which illustrates a gradual increase in mI_{CAT} after break-through (triangle) when the pipette solution contained 200 μM GTPγS. Holding potential was −40 mV; voltage steps to −120 mV (1.2-s duration) and slow voltage ramps from 80 to −120 mV (6-s duration) were applied at 20-s intervals as seen by the vertical deflections. The ramp pulses were long enough to obtain steady-state I-V relationships as was verified by increasing the duration of the voltage ramp to 24 s (not depicted). The dashed line indicates zero current level. (B) Superimposed I-V relationships measured in this experiment. Note that at positive potentials, mI_{CAT} increases and saturates progressively faster (Bolton and Zholos, 2003). For example, in the sixth trace mI_{CAT} reached 92% of the maximum at 80 mV, whereas at −120 mV by this time the current reached only 32% of its saturation level (first two traces superimpose at negative potentials). The same behavior was observed when agonist concentration was increased in steps (not depicted). (C) Cationic conductance activation curves obtained by dividing current amplitude at each potential by the driving force at that potential. The curves were fitted by Eq. 2. The fit range was restricted to negative potentials, i.e., the range negative to about −40 mV before channel flicker block reduced cationic conductance. (D) Parameters of the activation curves plotted against time of the GTPγS action. Note that G_{max} and $V_{1/2}$ values change in a similar way while the slope factor remains much the same, on average −19.7 ± 1.7 mV (n = 13). The SEM values are not shown as they were smaller than the size of symbols.

equation similar to Eq. 4 (P_O substituted for by relative conductance; not depicted). This allowed an estimate of the gating charge, which was found to be 1.4 ± 0.2e (n = 13) as well as the value of L(0) = 0.134 ± 0.017 (n = 13). These values predict intrinsic gating of the channel in the absence of ligands with $V_{1/2}$ = −36 mV. It can be speculated that the variable and more negative starting value of the $V_{1/2}$ depends on the amount of spontaneous coupling between constitutively active muscarinic receptors (and possibly other GPCRs) and their associated G-proteins.

DISCUSSION

Channel States

Although three types of cation channel were observed upon muscarinic receptor activation in single patches, or during the action of GTPγS, there seems little doubt that the 57-pS cation channel studied here is the major contributor to the cation current observed in response to muscarinic receptor activation of longitudinal intestinal smooth muscle cells (Benham et al., 1985; Zholos and Bolton, 1994). On the one hand the 130-pS channel did not show the required voltage-dependent behavior typical of whole-cell mI_{CAT} as its integral patch current was almost a linear function of the membrane potential. When $[Ca^{2+}]_i$ was clamped at 500 nM ~50% of mI_{CAT} was insensitive to voltage and it is likely that the 130-pS channel is the main contributor to this component (Tsytsyura et al., 2000; Zholos et al., 2003). The 10-pS channel was often seen but calculations showed its contribution to whole-cell current could seldom exceed 5% at negative potentials. The 57-pS channel on the other hand showed many of the characteristics of mI_{CAT}: its voltage dependence closely resembled that of mI_{CAT}, and the double rectification of mI_{CAT} around 0 mV (in symmetrical Cs^+ solutions) could be attributed to the flicker block of the 57-pS channel in this potential region, so it seems clear that this channel contributes most of the current to mI_{CAT} under normal circumstances. However, other features such as the sensitivity to $[Ca^{2+}]_i$, have yet to be explored in detail.

The density of the 57-pS channel in the membrane can be estimated. Previous noise analysis of the whole-cell current suggested a mean maximal P_O at −40 mV of 0.48 ± 0.05 and the number of channels to be 749 ± 76 (n = 9) (Zholos et al., 2003). This P_O value is consistent with the present single-channel measurements (Table I), whereas the number of channels can now be estimated more directly by taking into account the average whole-cell cationic conductance of 20.4 nS (from 1,020 ± 66 pA average current activated by 50 μM carbachol application at −50 mV, n = 112; Yan et al., 2003), a single-channel conductance of 57 pS and P_O = 0.43. These values predict 832 channels, or 1 channel

Published April 26, 2004

per 6.45 μ^2 as the average membrane capacitance is 53.7 ± 1.2 pF (n = 112).

Low-channel density and their significant clustering can explain why 61% of outside-out patches were blank. Average cation channel density is ~0.2 μ^{-2}. Clearly channels are not evenly distributed over the cell surface as two thirds of patches were without channel activity although it is conceivable that channels in blank patches are simply inactive for some reason. However, one fifth of patches were encountered with two to seven active channels, so clearly clustering of active channels occurs. This may reflect structural arrangements, such that channels are inserted only in certain regions, or equally it may suggest that channel activity reflects localization of channel-activating factors.

However, it remains to be explained why so few successful recordings were obtained when carbachol was applied in the pipette alone (0%) or to the cell in the conventional cell-attached patch configuration (5%), or when carbachol was applied after an outside-out patch has been formed (9%) as opposed to when carbachol was applied before first forming an outside-out patch (30%). Our suggestion at present is that loss of phosphatidylinositol 4,5,bisphosphate (PIP_2) from the membrane when M3 receptors are activated is crucial for the mI_{CAT} response and opening of the 57-pS channels, so prior depletion of PIP_2 is necessary for M2 receptor activation to be effective. There are four times as many M_2 as M_3 receptors, so that in cell-attached patches the numbers of M_3 receptors may be insufficient to produce the required threshold depletion of PIP_2 and activation of mI_{CAT} upon M_2 receptor stimulation. Outside-out patches are bigger than inside-out or cell-attached patches so the paucity of M_3 receptors may not be so limiting; thus, carbachol activated channels in 9% of outside-out patches. GTPγS will deplete PIP_2 directly, independently of M_3 stimulation so would be expected, as found, to be more reliable in evoking mI_{CAT}. The coupling of receptor stimulation to mI_{CAT} does not seem to involve any diffusible factors as 57-pS channel activity was remarkably persistent in isolated patches.

Our previous whole-cell experiments have showed the involvement of both the M_2/Gαo system (Yan et al., 2003) and the M_3/PLC system without significant participation of either $InsP_3$, DAG, or Ca^{2+} store depletion (Zholos et al., 2004). The proposed mI_{CAT} TRP connection (Walker et al., 2001; Lee et al., 2003) is consistent with PLC-dependent signaling (for review see Clapham, 2003) as the two main PLC metabolites also do not activate TRPC4 and TRPC5 proteins, while heterologous expression studies showed they have remarkably similar I-V relationships and single-channel activity patterns (Schaefer et al., 2002; for review see Clapham, 2003) to the 57-pS channel we observe.

The most impressive characteristic of the 57-pS channel was the relationship of long closings and short openings, and vice versa; this reciprocal relationship extended throughout the open/closed time ranges (Fig. 6 C) and indicates a model of the channel with pairs of open-closed states so that the greater probability would be that the channel transitions within open-closed state pairs. This follows from the high degree of negative correlation between the durations of open and closed states, which indicates more than a single pathway between open states (connectivity greater than unity, see Colquhoun and Hawkes, 1995) and excludes linear schemes where connectivity is unity.

Recordings showed a highly heterogeneous distribution of the probabilities of the open state (Figs. 8 B and 9 A). Horizontal transitions according to Scheme I are likely to be the main cause of the oscillatory behavior of P_O, which could not be attributed to some artifact of the signal averaging procedure (Figs. 1 D, 8 D, and 9, B and C). Intervals where P_O approached unity were characterized by a series of consecutive long openings characterized by the long dwell times of the O4 state (Fig. 9 C); conversely, when P_O within an interval was close to zero, such long openings were rare or absent, and the number of openings with the long O4 dwell time correlated well with the P_O of the interval (Fig. 8 A and Fig. 9 A, inset). Intervals of mixed gating resulting in a mean interval P_O of ~0.5 were also present (e.g., traces 3–5 and 9–10 in Fig. 9 C); the corresponding peak was particularly pronounced in Fig. 8 B, but when the mean P_O was lower the number of 5-s intervals with $P_O < 0.05$ became dominant (Fig. 9 A). The explanation of these oscillations in P_O with a P_O-dependent frequency is at present obscure.

For the K_{ACh} channel gated by the Gβγ subunit, different frequency of openings encoded P_O modes (Ivanova-Nikolova et al., 1998), but in the case of the muscarinic cation channel gated by Gαo-GTP in a PLC-dependent manner, the increase of P_O results from more frequent transitions into C4-O4 gating. It is characterized by very long, up to 1 s channel openings (Fig. 9 C), which suggest the existence of relatively stable complexes. However, the frequency limitations of the recording method means that there may be some unsuspected short-lived states (with the time constants <100 μs) that are undetectable, thus producing more than the four pairs of states that we have resolved. In addition, there must be more states of the channel since inactivation of mI_{CAT} at very positive potentials has been observed in whole-cell recordings from which no or very little recovery was possible (Zholos et al., 2003). In single-channel experiments this was seen as an abrupt loss of channel activity without obvious prior alteration in channel kinetics. At present there is no evidence how this inactivated/desensitized state(s) is re-

Published April 26, 2004

lated to the four postulated pairs of open-closed states. Channel flicker block seen at positive potentials is also not formally represented in our Scheme I, which is therefore applicable only to potentials in the negative range. Our scheme thus represents the most parsimonious one, as, with many more than the 10,000 or so events which we were able to analyze, more than four pairs of open-closed states may have been detected, as well as other embellishments of our model.

Effects of Membrane Potential on Channel Gating

Membrane depolarization caused a significant increase of channel P_O (Fig. 12 A). According to the 8-state Markov chain (Scheme I), several different changes in channel gating could potentially contribute to this effect: (a) shortening of channel shuttings, which is equivalent to increased frequency of openings; (b) prolongation of openings, which could be accompanied conversely by the reduction of their frequency; and (c) shifting of the gating such that channel states on the right of the scheme become more populated, i.e., relative contributions of C4 and O4 states increase. However, the latter effect was not observed as voltage had no or little effect on the relative times spent in the four postulated pairs of open-closed states (Fig. 10) implying that potential does not much affect the horizontal equilibrium in Scheme I. Channel P_O was a sigmoid function of potential (Fig. 12 A) mainly due to a change in channel mean closed time (Fig. 12 C) and some change in channel mean open time positive to −40 mV (Fig. 12 B). The latter effect argues for some greater effect on open-closed transition rates, or on the longest opening/shortest closing pair of states.

Cationic Channel Ligands and Whole-cell Current Predictions

The 57-pS channel showed a very low P_O in the absence of receptor activation in some recordings in symmetrical Cs^+ solutions; in physiological ion gradients this P_O is likely to be even lower (Kang et al., 2001). Activation of the muscarinic receptors or G-proteins greatly increased P_O and long openings correlated well with open probability (Figs. 8 A and 9 A, inset). There is an implication that G-protein binding to the channel affects transitions between, rather than within, pairs of open-closed states. However, this was not tested in the present experiments by applying different concentrations of carbachol for example, or recording channel activity as the effects of GTPγS develop. If $[Ca^{2+}]_i$ is buffered to very low levels then mI_{CAT} does not develop or is exceedingly small (Inoue and Isenberg, 1990c), indicating that most likely the cation channels are virtually fixed in the longest closed state under these conditions and that raising $[Ca^{2+}]_I$ affects transitions between channel pairs toward those with longer open times. Further work will be needed to test this prediction. However, the results of our analysis of changes of the whole-cell I-V relationships (Fig. 13) with reference to Scheme I are generally consistent with the hypothesis that along with accumulation of activated G-proteins there is a horizontal gating shift toward C4-O4 pair of states.

The cation channel probably exists as part of a complex with a number of other types of molecule. Two key molecules that are involved in cation channel opening, Gαo (Yan et al., 2003) and PLCβ (Zholos et al., 2004), are attached to the membrane via lipid modification (Hamm, 1998) and pleckstrin homology domains (Philip et al., 2002). The absence of these and other cofactors for channel opening may render inactive otherwise potentially active channels. The observation that both M_2 and M_3 subtypes of muscarinic receptor are required for channel opening (Zholos and Bolton, 1997; Bolton and Zholos, 2003; Unno et al., 2003) may suggest that a heterocomplex of these with the G-protein, cation channel, and other cofactors may exist.

In conclusion, the main strength of the channel scheme we suggest is that it accounts for the strong inverse relationship between open and closed time durations. It does not, however, take account of desensitization, inactivation or flicker block, and is limited by the inability of the recording system to detect events <0.1 ms. Changes in potential do not seem to alter the transitions between pairs of open-closed states much, having their major effect on the rates of transitions within pairs, particularly the longest opening-shortest closing pair of states. As for the effects of $[Ca^{2+}]_i$ and G-proteins, our scheme predicts these should favor longer-lived open states by affecting transitions between pairs of open-closed states and further work will be needed to test this possibility.

This work was supported by a grant to T.B. Bolton and A.V. Zholos from The Wellcome Trust (062926).

Lawrence G. Palmer served as editor.

Submitted: 22 December 2003
Accepted: 29 March 2004

REFERENCES

Altomare, C., A. Bucchi, E. Camatini, M. Baruscotti, C. Viscomi, A. Moroni, and D. DiFrancesco. 2001. Integrated allosteric model of voltage gating of HCN channels. *J. Gen. Physiol.* 117:519–532.

Benham, C.D., T.B. Bolton, and R.J. Lang. 1985. Acetylcholine activates an inward current in single mammalian smooth muscle cells. *Nature.* 316:345–347.

Bolton, T.B., and A.V. Zholos. 1997. Activation of M_2 muscarinic receptors in guinea-pig ileum opens cationic channels modulated by M_3 muscarinic receptors. *Life Sci.* 60:1121–1128.

Bolton, T.B., and A.V. Zholos. 2003. Potential synergy: voltage-driven steps in receptor-G protein coupling and beyond. *Sci. STKE*:pe52.

Clapham, D.E. 2003. TRP channels as cellular sensors. *Nature.* 426:

517–524.

Colquhoun, D. 1998. Binding, gating, affinity and efficacy: the interpretation of structure-activity relationships for agonists and of the effects of mutating receptors. *Br. J. Pharmacol.* 125:924–947.

Colquhoun, D., and A.G. Hawkes. 1995. The principles of the stochastic interpretation of ion-channel mechanism. *In* Single-channel Recording. B. Sakmann and E. Neher, editors. Plenum Press, New York. 397–482.

Colquhoun, D., and B. Sakmann. 1998. From muscle endplate to brain synapses: A short history of synapses and agonist-activated ion channels. *Neuron.* 20:381–387.

Cox, D.H., J. Gui, and R.W. Aldrich. 1997. Allosteric gating of a large conductance Ca-activated K^+ channel. *J. Gen. Physiol.* 110: 257–281.

del Castillo, J., and B. Katz. 1957. Interaction at end-plate receptors between different choline derivatives. *Proc. R. Soc. B.* 146:369–381.

Edmonds, B., A.J. Gibb, and D. Colquhoun. 1995. Mechanisms of activation of muscle nicotinic acetylcholine receptors and the time course of endplate currents. *Annu. Rev. Physiol.* 57:469–493.

Eglen, R.M., S.S. Hegde, and N. Watson. 1996. Muscarinic receptor subtypes and smooth muscle function. *Pharmacol. Rev.* 48:531–565.

Gilman, A.G. 1987. G proteins: transducers of receptor-generated signals. *Annu. Rev. Biochem.* 56:615–649.

Gordienko, D.V., A.V. Zholos, and T.B. Bolton. 1999. Membrane ion channels as physiological targets for local Ca^{2+} signalling. *J. Microsc.* 196:305–316.

Hamm, H.E. 1998. The many faces of G protein signaling. *J. Biol. Chem.* 273:669–672.

Inoue, R., and G. Isenberg. 1990a. Acetylcholine activates nonselective cation channels in guinea pig ileum through a G protein. *Am. J. Physiol.* 258:C1173–C1178.

Inoue, R., and G. Isenberg. 1990b. Effect of membrane potential on acetylcholine-induced inward current in guinea-pig ileum. *J. Physiol.* 424:57–71.

Inoue, R., and G. Isenberg. 1990c. Intracellular calcium ions modulate acetylcholine-induced inward current in guinea-pig ileum. *J. Physiol.* 424:73–92.

Inoue, R., K. Kitamura, and H. Kuriyama. 1987. Acetylcholine activates single sodium channels in smooth muscle cells. *Pflugers Arch.* 410:69–74.

Ivanova-Nikolova, T.T., and G.E. Breitwieser. 1997. Effector contributions to Gβγ-mediated signaling as revealed by muscarinic potassium channel gating. *J. Gen. Physiol.* 109:245–253.

Ivanova-Nikolova, T.T., E.N. Nikolov, C. Hansen, and J.D. Robishaw. 1998. Muscarinic K^+ channel in the heart. Modal regulation by G protein βγ subunits. *J. Gen. Physiol.* 112:199–210.

Kang, T.M., Y.C. Kim, J.H. Sim, J.C. Rhee, S.J. Kim, D.Y. Uhm, I. So, and K.W. Kim. 2001. The properties of carbachol-activated nonselective cation channels at the single channel level in guinea pig gastric myocytes. *Jpn. J. Pharmacol.* 85:291–298.

Komori, S., and T.B. Bolton. 1990. Role of G-proteins in muscarinic receptor inward and outward currents in rabbit jejunal smooth muscle. *J. Physiol.* 427:395–419.

Komori, S., M. Kawai, P. Pacaud, H. Ohashi, and T.B. Bolton. 1993. Oscillations of receptor-operated cationic current and internal calcium in single guinea-pig ileal smooth muscle cells. *Pflugers Arch.* 424:431–438.

Lee, Y.M., B.J. Kim, H.J. Kim, D.K. Yang, M.H. Zhu, K.P. Lee, I. So, and K.W. Kim. 2003. TRPC5 as a candidate for the nonselective cation channel activated by muscarinic stimulation in murine stomach. *Am. J. Physiol.* 284:G604–G616.

McManus, O.B., A.L. Blatz, and K.L. Magleby. 1985. Inverse relationship of the durations of adjacent open and shut intervals for Cl and K channels. *Nature.* 317:625–627.

Nilius, B. 2003. Calcium-impermeable monovalent cation channels: a TRP connection? *Br. J. Pharmacol.* 138:5–7.

Pacaud, P., and T.B. Bolton. 1991. Relation between muscarinic receptor cationic current and internal calcium in guinea-pig jejunal smooth muscle cells. *J. Physiol.* 441:477–499.

Pallotta, B.S. 1997. Kinetic models of ion channels. *Ann. NY Acad. Sci.* 812:133–140.

Petit-Jacques, J., J.L. Sui, and D.E. Logothetis. 1999. Synergistic activation of G protein-gated inwardly rectifying potassium channels by the βγ subunits of G proteins and Na^+ and Mg^{2+} ions. *J. Gen. Physiol.* 114:673–684.

Philip, F., Y. Guo, and S. Scarlata. 2002. Multiple roles of pleckstrin homology domains in phospholipase Cβ function. *FEBS Lett.* 531: 28–32.

Schaefer, M., T.D. Plant, N. Stresow, N. Albrecht, and G. Schultz. 2002. Functional differences between TRPC4 splice variants. *J. Biol. Chem.* 277:3752–3759.

Smith, S.W. 1997. The Scientist and Engineer's Guide to Digital Signal Processing. California Technical Publishing, San Diego, CA. 626 pp.

Tsytsyura, Y.D., A.V. Zholos, M.F. Shuba, and T.B. Bolton. 2000. Effects of intracellular Ca^{2+} on muscarinic cationic current in guinea pig ileal smooth muscle cells. *Neurophysiology.* 32:236–237.

Unno, T., H. Matsuyama, and S. Komori. 2003. Interaction between the M_2- and M_3-receptor subtypes in muscarinic electrical and mechanical responses of intestinal smooth muscles. *Neurophysiology.* 35:290–301.

Walker, R.L., J.R. Hume, and B. Horowitz. 2001. Differential expression and alternative splicing of TRP channel genes in smooth muscles. *Am. J. Physiol.* 280:C1184–C1192.

Wang, Y.X., B.K. Fleischmann, and M.I. Kotlikoff. 1997. M_2 receptor activation of nonselective cation channels in smooth muscle cells: Calcium and G_i/G_0 requirements. *Am. J. Physiol.* 273:C500–C508.

Wickman, K., and D. Clapham. 1995. Ion channel regulation by G proteins. *Physiol. Rev.* 75:865–885.

Yan, H.D., H. Okamoto, T. Unno, Y.D. Tsytsyura, S.A. Prestwich, S. Komori, A.V. Zholos, and T.B. Bolton. 2003. Effects of G-protein-specific antibodies and Gβγ subunits on the muscarinic receptor-operated cation current in guinea-pig ileal smooth muscle cells. *Br. J. Pharmacol.* 139:605–615.

Zholos, A.V., and T.B. Bolton. 1994. G-protein control of voltage dependence as well as gating of muscarinic metabotropic channels in guinea-pig ileum. *J. Physiol.* 478:195–202.

Zholos, A.V., and T.B. Bolton. 1996. A novel GTP-dependent mechanism of ileal muscarinic metabotropic channel desensitization. *Br. J. Pharmacol.* 119:997–1012.

Zholos, A.V., and T.B. Bolton. 1997. Muscarinic receptor subtypes controlling the cationic current in guinea-pig ileal smooth muscle. *Br. J. Pharmacol.* 122:885–893.

Zholos, A.V., V.V. Tsvilovskyy, and T.B. Bolton. 2003. Muscarinic cholinergic excitation of smooth muscle: signal transduction and single cationic channel properties. *Neurophysiology.* 35:283–301.

Zholos, A.V., Y.D. Tsytsyura, D.V. Gordienko, V.V. Tsvilovskyy, and T.B. Bolton. 2004. Phospholipase C, but not $InsP_3$ or DAG, dependent activation of the muscarinic receptor-operated cation current in guinea-pig ileal smooth muscle cells. *Br. J. Pharmacol.* 141:23–36.